Mechanism for the inhibition of the cAMP dependence of HCN ion channels by the auxiliary subunit TRIP8b

Received for publication, June 5, 2017, and in revised form, August 29, 2017 Published, Papers in Press, September 1, 2017, DOI 10.1074/jbc.M117.800722

John R. Bankston[‡1], Hannah A. DeBerg[‡§], Stefan Stoll[§], and William N. Zagotta[‡2]

From the Departments of [‡]Physiology and Biophysics and [§]Chemistry, University of Washington, Seattle, Washington 98195

Edited by Roger J. Colbran

TRIP8b, an accessory subunit of hyperpolarization-activated cyclic nucleotide-gated (HCN) ion channels, alters both the cell surface expression and cyclic nucleotide dependence of these channels. However, the mechanism by which TRIP8b exerts these dual effects is still poorly understood. In addition to binding to the carboxyl-terminal tripeptide of HCN channels, TRIP8b also binds directly to the cyclic nucleotide-binding domain (CNBD). That interaction, which requires a small central portion of TRIP8b termed TRIP8b$_{core}$, is both necessary and sufficient for reducing the cAMP-dependent regulation of HCN channels. Here, using fluorescence anisotropy, we report that TRIP8b binding to the CNBD of HCN2 channels decreases the apparent affinity of cAMP for the CNBD. We explored two possible mechanisms for this inhibition. A noncompetitive mechanism in which TRIP8b inhibits the conformational change of the CNBD associated with cAMP regulation and a competitive mechanism in which TRIP8b and cAMP compete for the same binding site. To test these two mechanisms, we used a combination of fluorescence anisotropy, biolayer interferometry, and double electron-electron resonance spectroscopy. Fitting these models to our fluorescence anisotropy binding data revealed that, surprisingly, the TRIP8b-dependent reduction of cAMP binding to the CNBD can largely be explained by partial competition between TRIP8b and cAMP. On the basis of these findings, we propose that TRIP8b competes with a portion of the cAMP-binding site or distorts the binding site by making interactions with the binding pocket, thus acting predominantly as a competitive antagonist that inhibits the cyclic-nucleotide dependence of HCN channels.

Electrical activity in cells throughout the body requires the precisely regulated opening and closing of ion channels. This tuning of ion channel function can occur in many ways, including the binding of ligands and through the association with accessory proteins. The opening of hyperpolarization-activated cyclic nucleotide-gated (HCN)[3] channels is enhanced by the direct binding of cAMP to a highly conserved cytoplasmic cyclic nucleotide-binding domain (CNBD) in each subunit (1). However, in neurons, this regulation of the channel function is mostly eliminated through the binding of the accessory subunit TRIP8b (2, 3).

TRIP8b is a highly alternatively spliced and primarily neuronal protein that can assemble with all mammalian HCN channels (2–6). In addition to reducing the cAMP dependence of HCN channels, TRIP8b regulates the cell surface expression in an isoform-dependent manner (2, 3, 6). TRIP8b has been shown to co-localize with HCN1 in the distal dendrites of hippocampal pyramidal neurons, and knocking out TRIP8b dramatically disrupts this dendritic localization (4, 5).

TRIP8b has a bipartite interaction with the carboxyl-terminal region of HCN channels. One binding interface for these two proteins involves a series of tetratricopeptide repeats (TPRs) on TRIP8b and the carboxyl-terminal residues of HCN channels (2, 3, 7, 8). The interaction has been elucidated in atomic detail with X-ray crystallography and is thought to be a high-affinity site that anchors these two proteins together (8).

The other binding interface involves the binding of a small segment of TRIP8b that has been termed TRIP8b$_{core}$ (residues 223–303) to the CNBD of HCN channels (4, 5, 9, 10). Patch clamp experiments utilizing only this TRIP8b$_{core}$ domain showed that it is both necessary and sufficient to inhibit the cAMP dependence of these channels (9, 10). This interface between the CNBD and TRIP8b$_{core}$ has been localized using double electron-electron resonance (DEER) and NMR spectroscopy (10, 11). The interface involves regions on the CNBD that are critical for cAMP binding, as well as regions critical for the conformational change that occurs subsequent to cAMP binding.

Although it is known that TRIP8b reduces the cAMP dependence of the channel gating, there is still debate as to the mechanism of this regulation. Biochemical data utilizing pulldown assays showed that increasing the concentration of cAMP or

This work was supported by NEI, National Institutes of Health Grants R01EY010329 (to W. N. Z. and S. S.) and K99EY024267 (to J. R. B.) and American Heart Association Grant 14CSA20380095 (to W. N. Z. and S. S.). Additional support was provided by the University of Washington (to S. S.) and from the Sackler Scholars Program in Integrative Biophysics (to H. A. D.). The authors declare that they have no conflicts of interest with the contents of this article. The content is solely the responsibility of the authors and does not necessarily represent the official views of the National Institutes of Health.

This article contains supplemental Figs. S1 and S2.

[1] Present address: Dept. of Physiology and Biophysics, University of Colorado Anschutz Medical Campus, Aurora, CO 80045.

[2] To whom correspondence should be addressed: Dept. of Physiology and Biophysics, Box 357290, University of Washington, Seattle, WA 98195-7290. Tel.: 206-685-3878; Fax: 206-543-0934; E-mail: zagotta@uw.edu.

[3] The abbreviations used are: HCN, hyperpolarization-activated cyclic nucleotide-gated; CNBD, cyclic nucleotide binding domain; DEER, double electron-electron resonance; TRIP8b, tetratricopeptide repeat-containing Rab8b-interacting protein; TPR, tetratricopeptide; Ni-NTA, nickel-nitrilotriacetic acid; MTSL, *S*-(1-oxyl-2,2,5,5-tetramethyl-2,5-dihydro-1*H*-pyrrol-3-yl)methyl methanesulfonothioate; TEV, tobacco etch virus; mBBr, monobromobimane; 8-fluo-cAMP, 8-(2-[fluoresceinyl] aminoethylthio) adenosine-3′,5′-cyclic monophosphate.

mutating the cAMP-binding site both reduced the total TRIP8b pulled down by HCN channels (5). The authors concluded that this suggested a direct competition between TRIP8b and cAMP for binding to HCN channels. In contrast, Hu *et al.* (9) analyzed patch clamp experiments with a model that suggested a mechanism where TRIP8b does not directly compete with cAMP for the binding to the channel but instead acts through an allosteric mechanism to decrease the affinity of the CNBD for ligand. Recent NMR work from two labs showed similar binding interfaces between the CNBD and TRIP8b, but each study arrived at subtly distinct conclusions (10, 11). Both groups suggested that TRIP8b could be working through both a competitive and noncompetitive mechanism. However, the two studies differed in the precise structural hypothesis for this competition. Saponaro *et al.* (11) suggested that TRIP8b binding might work by inhibiting the conformational change associated with channel opening that takes place in the N-terminal region of the CNBD and allosterically reducing cAMP binding affinity. DeBerg *et al.* (10) hypothesized a partial overlap of the binding sites for TRIP8b and cAMP and inhibition of a different conformational change in the C-helix that is associated with cAMP binding.

Given this uncertainty, we set out to determine whether TRIP8b acts as a competitive antagonist or noncompetitive antagonist of HCN channels. We used fluorescence anisotropy and biolayer interferometry to quantify the binding affinities of cAMP and TRIP8b for the isolated CNBD of HCN2. In addition, we utilized DEER to quantify the extent to which cAMP and TRIP8b regulate the activation conformational change of the CNBD. With these data, we were able to test the two mechanisms by fitting the data to models for competitive and noncompetitive mechanisms of inhibition. We found that, surprisingly, a partially competitive mechanism, but not a noncompetitive mechanism, was sufficient to explain the TRIP8b inhibition in cAMP binding.

Results

TRIP8b$_{core}$ inhibits cAMP-dependent regulation of HCN2 channels

TRIP8b is a cytosolic protein composed of three primary domains (Fig. 1*A*). The first is the variable N-terminal domain that is the site of alternative splicing. The second is a small central domain comprised of 80 amino acids called TRIP8b$_{core}$, which contains a conserved region that is present in all orthologs of TRIP8b, as well some flanking sequence on both the amino- and carboxyl-terminal sides of the protein. The last is a carboxyl-terminal series of six TPR repeats that binds to the terminal amino acids at the carboxyl terminus of HCN channels (Fig. 1*B*). Recent work has shown that TRIP8b$_{core}$ binds to the CNBD near a critical mobile helix called the C-helix, which changes conformation in response to cAMP binding (Fig. 1*B*) (10, 11). This binding virtually eliminates the cAMP-dependent regulation of HCN2 channels (9, 10, 12). Here, we confirmed that effect by applying purified TRIP8b$_{core}$ to inside-out excised patches from *Xenopus laevis* oocytes expressing HCN2 channels. In the absence of TRIP8b, 1 μM cAMP dramatically increased the rate and extent of channel opening and shifted the voltage dependence of activation to more depolarized levels

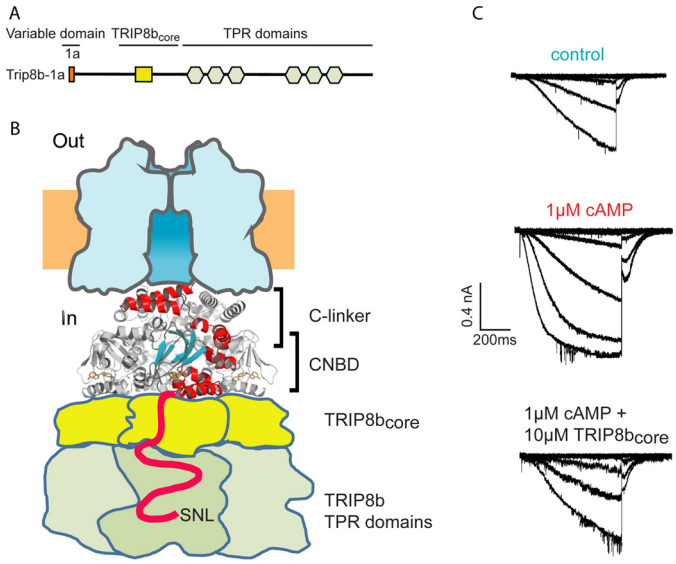

Figure 1. TRIP8b inhibits the cAMP dependence of HCN2 channels. *A*, schematic cartoon showing the major domains of TRIP8b. The *orange rectangle* represents the variable domain 1a. The *yellow rectangle* represents a conserved region that is absolutely conserved in all orthologs of TRIP8b. The *light green hexagons* represent the individual TPRs that make up the TPR domain. *B*, cartoon showing TRIP8b interacting with the carboxyl-terminal region of HCN channels. The structure of the C-linker/CNBD is adapted from PDB 1Q43 (30). *C*, representative current traces elicited by stepping the voltage to hyperpolarized potentials between −70 and −140 mV in inside-out patches from oocytes expressing HCN2 channels. The *top panel* shows currents in the absence of ligand, the *middle panel* is in the presence of 1 μM cAMP, and the *bottom panel* is in the presence of both 1 μM cAMP and 10 μM TRIP8b.

(Fig. 1*C*). However, perfusing both 1 μM cAMP and 10 μM TRIP8b onto the patch resulted in currents that were nearly identical to control currents.

cAMP and TRIP8b$_{core}$ bind the CNBD

To understand the mechanism of TRIP8b inhibition of the cAMP dependence of HCN channels, we measured the binding affinities of both cAMP and TRIP8b for the CNBD. To do this, we used a fragment of the HCN2 CNBD that contains the CNBD and helices C′ through F′ of the C-linker (residues 488–640) termed HCN2-CNBDxt. We have previously shown that this fragment of HCN2 is able to bind cAMP and undergo the conformational change associated with cyclic nucleotide binding (10). Compared with the larger cytosolic fragment that contains both the CNBD and the full C-linker, HCN2-CNBDxt lacks the region required for domain tetramerization and is more soluble when in complex with TRIP8b.

To determine the apparent affinity of cAMP for the CNBD, we measured the anisotropy of 20 nM 8-fluo-cAMP, a fluorescent analog of cAMP, with increasing amounts of HCN2-CNBDxt. Fluorescence anisotropy was then plotted *versus* total concentration of HCN2-CNBDxt, and the data were fit with a single binding isotherm (see "Experimental procedures," Equation 2) (Fig. 2*A*). This revealed an apparent binding affinity for HCN2-CNBDxt and 8-fluo-cAMP of 324 ± 88 nM (n = 3).

To determine the binding affinity for TRIP8b$_{core}$ and HCN2-CNBDxt, we labeled TRIP8b$_{core}$ with the fluorophore bimane. To do this, position Ala-261 of TRIP8b$_{core}$ was mutated to cys-

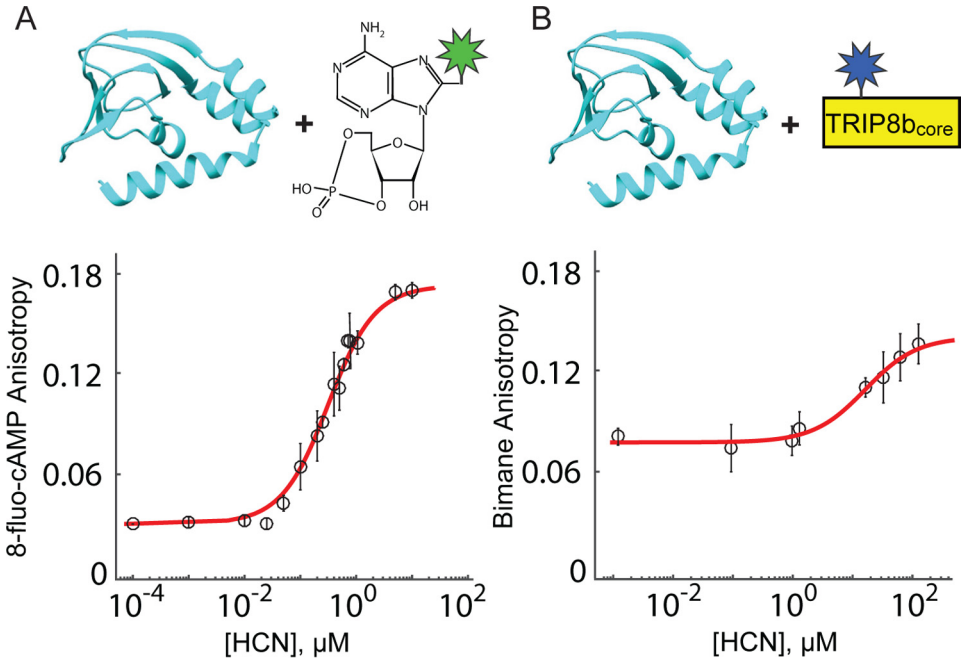

Figure 2. TRIP8b and cAMP both bind to HCN2-CNBDxt. *A*, fluorescence anisotropy measurements of a fluorescent analog of cAMP (8-fluo-cAMP) plotted *versus* the total concentration of HCN2-CNBDxt ($n = 3$). These data were fit with Equation 2 to give an apparent binding affinity of 324 ± 88 nM. *B*, fluorescence anisotropy measurements of a bimane-labeled TRIP8b$_{core}$ plotted *versus* the total concentration of HCN2-CNBDxt ($n = 3$). These data were fit with Equation 2 to give an apparent binding affinity of 8.4 ± 4.1 μM. The data are plotted as means ± S.E.

teine, and that position was labeled using monobromobimane. We previously labeled this position with MTS spin labels for EPR experiments and showed that the labeled TRIP8b still bound to the CNBD of HCN channels (10). The anisotropy of the labeled TRIP8b$_{core}$ (50 nM) was then measured in different amounts of HCN2-CNBDxt. These data were plotted and fit with a single binding isotherm (Equation 2), which showed a binding affinity of 8.4 ± 4.1 μM ($n = 3$) (Fig. 2*B*).

As an additional assay for TRIP8b binding, we utilized biolayer interferometry, which analyzes the shift in interference pattern as one protein binds to a fiber optic biosensor prebound with an immobilized second protein. This method allowed us to measure not only the affinity of the interaction, but also the rates of binding and unbinding. Another advantage of this approach is that it uses wild-type unlabeled proteins, eliminating the possibility that the fluorescent label could be affecting binding. To measure binding of TRIP8b$_{core}$ to HCN2-CNBDxt, we immobilized an N-terminally His-tagged HCN2-CNBDxt onto a row of eight biosensors that are coated with Ni-NTA. The biosensors were then dipped into a 96-well plate with wells that contain varying concentrations of TRIP8b$_{core}$, which allowed for the measurement of binding (on) rates (Fig. 3*A*, *left panel*). The sensor was then moved to a well that contained buffer only and the unbinding (off) rates were determined (Fig. 3*A*, *right panel*).

A representative set of binding curves is shown in Fig. 3*B*. We first used Equation 3 to fit these data. We made k_{on} and k_{off} global fit parameters and determined the values that produced the best fit to all the TRIP8b$_{core}$ concentrations for a single preparation (Fig. 3*C*). Doing this with three different preparations of HCN2-CNBDxt and TRIP8b$_{core}$ resulted in a measured k_{on} of $1 \times 10^5 \pm 0.16 \times 10^5$ M^{-1} s^{-1} and k_{off} of 0.72 ± 0.14 s^{-1} ($n = 3$). From these data, K_d ($= k_{off}/k_{on}$) for the binding of TRIP8b$_{core}$ to HCN2-CNBDxt was 7.35 ± 1.3 μM ($n = 3$), similar to the value measured from anisotropy measurements.

As a second method for calculating the on and off rates, the binding data for each concentration of TRIP8b$_{core}$ were fit individually with Equation 4. The resulting k_{obs} from the fits were then plotted *versus* the concentration of TRIP8b$_{core}$ (Fig. 3*D*). As expected, k_{obs} was linearly related to protein concentration, and the data could be fit with Equation 5. The slope of this line gives a measurement of k_{on} (1.12×10^5 M^{-1} s^{-1}), whereas the *y* intercept gives k_{off} (0.73 s^{-1}). The K_d value (k_{off}/k_{on}) of 6.5 μM is in good agreement with the global fit calculation, as well as the anisotropy measurement. These data establish the rates of the binding and unbinding of TRIP8b$_{core}$ to HCN2-CNBDxt and demonstrate that the fluorophore labeling of TRIP8b$_{core}$ did not significantly affect binding to HCN2-CNBDxt.

TRIP8b inhibits binding of cAMP to HCN2

Functional studies have shown that TRIP8b reduces the apparent affinity of cAMP for activation of HCN channels (9, 10). We sought to determine the mechanism for this inhibition by directly measuring the binding of cAMP to HCN channels in the presence of TRIP8b. Again, we measured the fluorescence anisotropy of 8-fluo-cAMP at increasing concentrations of HCN2-CNBDxt. However, in this experiment, the measurements were made in the presence of increasing amounts of TRIP8b$_{core}$, and the data were normalized by subtracting the minimum anisotropy value from each data point and dividing by the maximum change in anisotropy. The results can be seen in Fig. 4*A*. The apparent affinity of cAMP binding to HCN2-CNBDxt decreases as the total concentration of TRIP8b increases.

To determine the mechanism of this inhibition of cAMP binding, we considered two models for the inhibition: noncom-

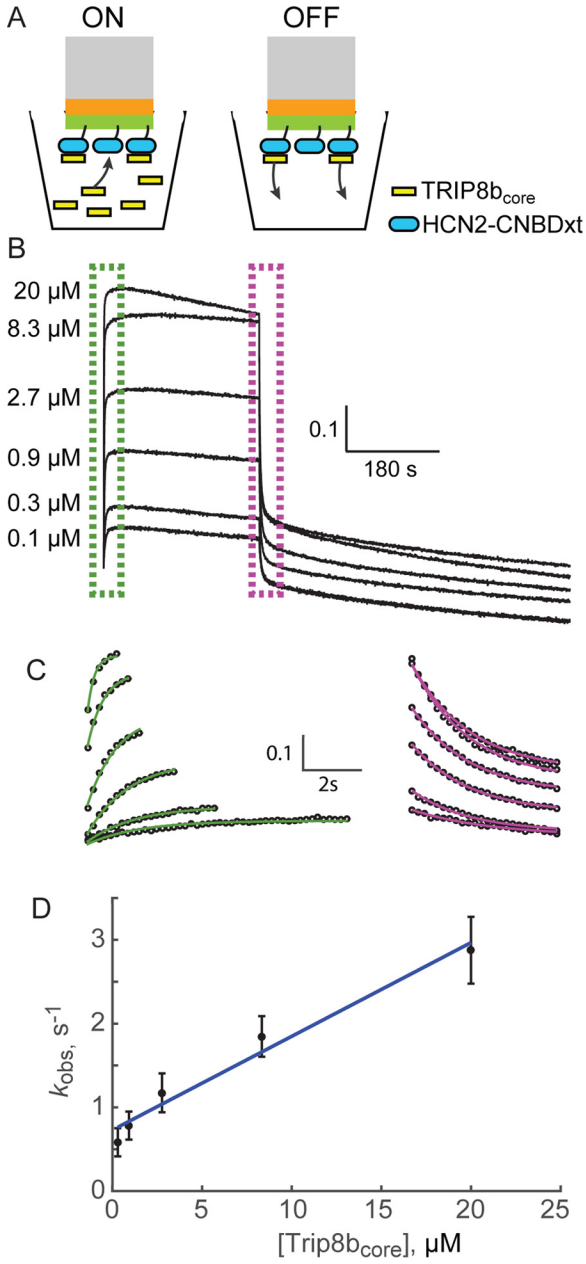

Figure 3. Biolayer interferometry reveals TRIP8b$_{core}$ affinity for HCN2-CNBDxt. *A*, cartoon representation of biolayer interferometry experiments. The *colored rectangle* represents the optical probe, and the *green* is the layer coated with Ni-NTA. The probes are loaded with HCN2-CNBDxt (*blue ovals*). The probe is then dipped into a well of a 96-well plate containing TRIP8b$_{core}$ (*yellow rectangles*). TRIP8b$_{core}$ binding kinetics are then measured. The probe is then moved to a well with only buffer, and TRIP8b$_{core}$ unbinding kinetics are measured. *B*, binding curves that show the shift in interference pattern of light as a function of time. This shift is directly related to the change in thickness of the optical layer, which is in turn related to the binding of TRIP8b$_{core}$. The concentration of TRIP8b$_{core}$ in the wells is indicated. *C*, the *boxed* regions from *B* are shown at an expanded time scale. These data are fit with Equation 3 revealing the on and off rates of TRIP8b binding. The average rates were $k_{on} = 1 \times 10^5 \pm 0.16 \times 10^5$ M^{-1} s^{-1} and $k_{off} = 0.72 \pm 0.14$ s^{-1} ($n = 3$). *D*, plot of k_{obs} *versus* the concentration of TRIP8b ($n = 3$). The slope of the linear fit to Equation 4 gives an estimate of k_{on} of 1.12×10^5 M^{-1} s^{-1}, and the *vertical intercept* estimates a k_{off} of 0.73 s^{-1}. These data are consistent with the global fits to the data in *B* and *C*. The data are plotted as means ± S.E.

petitive and partially competitive. In the first model, both cAMP and TRIP8b can bind to HCN2-CNBDxt simultaneously, but TRIP8b inhibits the conformational change associated with cAMP binding, (Fig. 4*B*). In the second model, TRIP8b and cAMP compete for binding to the CNBD (Fig. 4*C*). In other words, cAMP inhibits the initial binding of TRIP8b and vice versa, suggesting partial overlap in their binding sites. Fitting these models to the steady-state binding data in Fig. 4*A* required that we determine the equilibrium constants K_T, K_C, and L. The dissociation constant of TRIP8b$_{core}$ for the unbound CNBD (K_T) was taken from the global fits to the interferometry data (7.3 μM), but all three of our measurements of TRIP8b$_{core}$ binding were in such good agreement that the model predictions are unaffected by which value we used. The dissociation constant for cAMP for the resting state of HCN2-CNBDxt (K_C) was determined from fitting a three-state model resulting from the models in Fig. 4 (*B* and *C*) when [TRIP8b$_{core}$] = 0. As described previously, the normalized anisotropy data of 8-fluo-cAMP binding in the absence of Trip8b$_{core}$ were fit using Equation 2 and produced a K_d of 324 nM. This number reflects the apparent affinity of cAMP for HCN2-CNBDxt. To determine K_C, we can use this apparent affinity, as well as the equilibrium constant for the activation conformational change, and solve the equation $K_C = K_d^*(1 + L)$.

To determine L, the equilibrium constant for the activation conformational change in the CNBD with bound cAMP, we utilized DEER spectroscopy. DEER measures distance distributions between two spin labels attached to a protein. DEER works over distances between 15 and 80 Å. The distance distributions measured by DEER report multiple conformational states of a protein along with the steady-state probability that the protein adopts each conformation. From these measurements, we can calculate the equilibrium constant between different conformations.

To measure the equilibrium constant for the activation conformational change in the CNBD, we introduced a pair of cysteines into HCN2-CNBDxt and labeled the sites with the spin label *S*-(1-oxyl-2,2,5,5-tetramethyl-2,5-dihydro-1*H*-pyrrol-3-yl)methyl methanesulfonothioate (MTSL). For these experiments, we selected a residue in the β-roll (S563C) and a residue in the C-helix (A624C) of the CNBD that have been previously shown to report the conformational change in the CNBD associated with cAMP binding (10, 13, 14). Fig. 5*A* shows the positions of this pair of cysteines with spin labels attached. For each spin-labeled site, side-chain ensembles were predicted using the MMM rotamer library (15). We have previously shown that when cAMP binds to the CNBD, the C-helix moves closer to the β-roll by ≈9 Å (10, 13, 14). Here we performed a similar experiment by looking at the distance distribution between these two positions in the absence and presence of saturating (1 mM) 8-fluo-cAMP (Fig. 5*B*). In an attempt to trap the room temperature equilibrium conformational ensemble, samples were flash frozen by rapid placement into liquid nitrogen (16, 17). As with previous experiments, we observed a shift in the distance distribution to shorter distances associated with a conformational change from the resting to the active state. However, even in saturating 8-fluo-cAMP, a fairly substantial probability density exists in the longer distance conformation. This balance between the longer "resting" state and the shorter "active" state represents an equilibrium between these two conformations that exists even in the presence of saturating ligand.

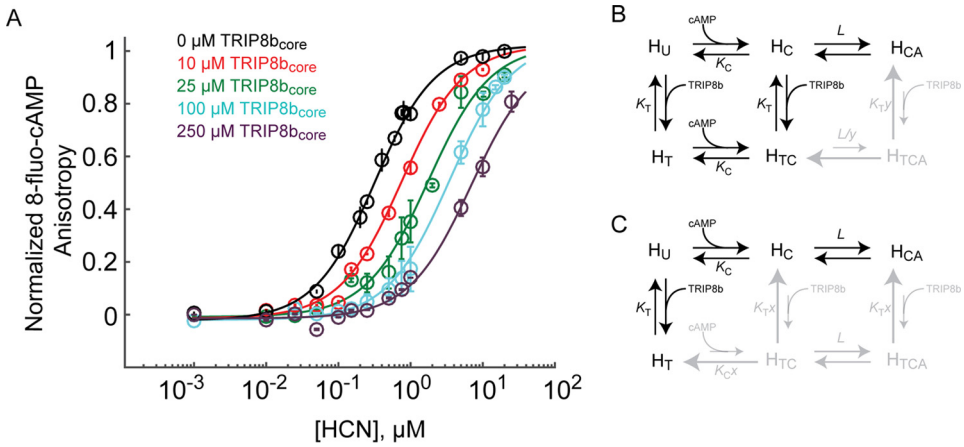

Figure 4. Data and models for TRIP8b inhibition of the cAMP dependence of HCN channels. *A*, normalized fluorescence anisotropy of 8-fluo-cAMP as a function of the total concentration of HCN2-CNBDxt in the presence of different concentrations of TRIP8b$_{core}$ ranging from 0 to 250 μM ($n = 4$). The data are plotted as means ± S.E. and fit with Equation 2. *B*, a noncompetitive model of TRIP8b inhibition of HCN channels where TRIP8b and cAMP can both bind (state H_{TC}), but once TRIP8b is bound, the conformational change associated with HCN2-CNBDxt activation is inhibited by a factor *y*. *Grayed out* states represent largely unpopulated states. *C*, a partially competitive model of TRIP8b inhibition of HCN channels where binding of TRIP8b inhibits binding of cAMP and vice versa by a factor of *x*. Again, *grayed out* states represent largely unpopulated states.

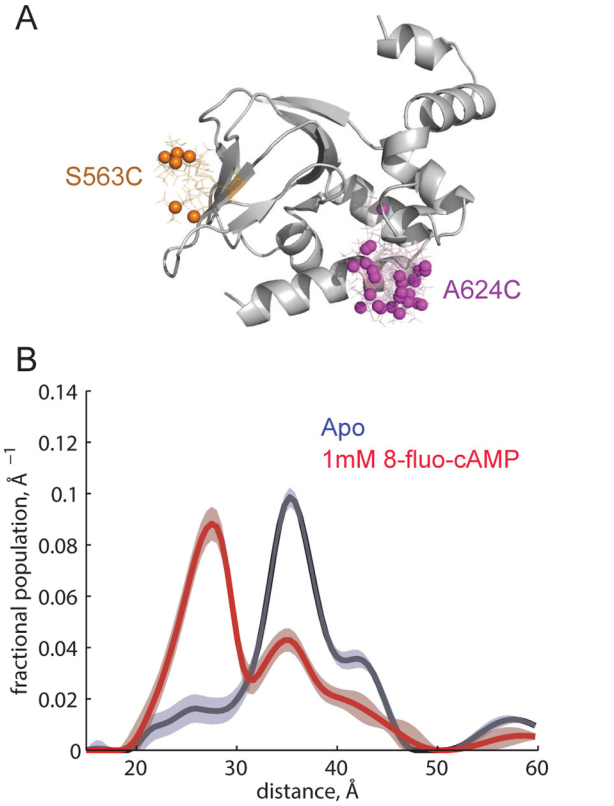

Figure 5. DEER reveals the equilibrium constant for the conformational change in the CNBD when bound to cAMP. *A*, HCN2-CNBDxt structure with spin-label rotamers at a position on the β-roll (S563C) and the C-helix (A624C). Rotameric models of MTSL attached to HCN2-CNBDxt were obtained using MMM (15). *B*, distance distributions of HCN2-CNBDxt S563C/A624C in the absence (*blue*) and presence (*red*) of 1 mM 8-fluo-cAMP.

To quantify this equilibrium, we measured the area under these peaks and calculated *L* by looking at the ratio of the areas under the activated *versus* resting components. The distance cutoff for discriminating active *versus* resting state was set at 31.5 Å. This resulted in a value for *L* of 1.3 ± 0.2 for 8-fluo-cAMP bound HCN2-CNBDxt, similar to the value determined for cAMP (13, 14, 18).

TRIP8b and cAMP compete for HCN channel binding

Using the previously determined equilibrium constants, we were then able to test our two models for TRIP8b inhibition of cAMP regulation. In the noncompetitive model in Fig. 6*A*, we assumed that TRIP8b only altered the resting-to-active conformational change after initial cAMP binding. In other words, the resting-state binding affinity of cAMP without and with TRIP8b$_{core}$ bound was the same (K_C), and the resting-state binding affinity of TRIP8b$_{core}$ without and with cAMP was the same (K_T). Only the equilibrium constant for the activation conformational change was different, decreased by TRIP8b$_{core}$ binding by a factor of *y* (*L versus L*/*y*). Surprisingly, even with a decrease in the equilibrium constant for activation by 4 orders of magnitude when TRIP8b$_{core}$ was bound ($y = 10{,}000$), the anisotropy data were not well fit by the purely noncompetitive model (Fig. 6*A*).

Alternatively, we tested the partial competition model by varying the dissociation constant for cAMP binding in the presence of TRIP8b while assuming that the conformational change subsequent to cAMP binding is unaffected. Fig. 6*B* shows that a 100-fold increase in the dissociation constant for cAMP binding in the presence of TRIP8b$_{core}$ ($x = 100$) is sufficient to fit the data well. A 100-fold effect on the equilibrium constant for binding is not complete competition but represents a 2.7 kcal/mol destabilization of cAMP binding in the presence of TRIP8b. Surprisingly, this suggests that partial competition for the binding site on the channel is sufficient to account for TRIP8b inhibition of the cAMP dependence of HCN channels. It is worth noting that using our models, we were only able to fit the data if TRIP8b$_{core}$ binding changed the cAMP affinity by at least 100-fold, even if it also changed the equilibrium constant for the conformational change. Supplemental Fig. S1 shows an example where we increased the dissociation constant for cAMP binding by 10-fold and decreased the equilibrium constant for the conformational change by 10-fold, and the data were still not fit well. Although this does not eliminate the possibility that TRIP8b could be affecting both the binding of cAMP and the conformational change, our results suggest, in

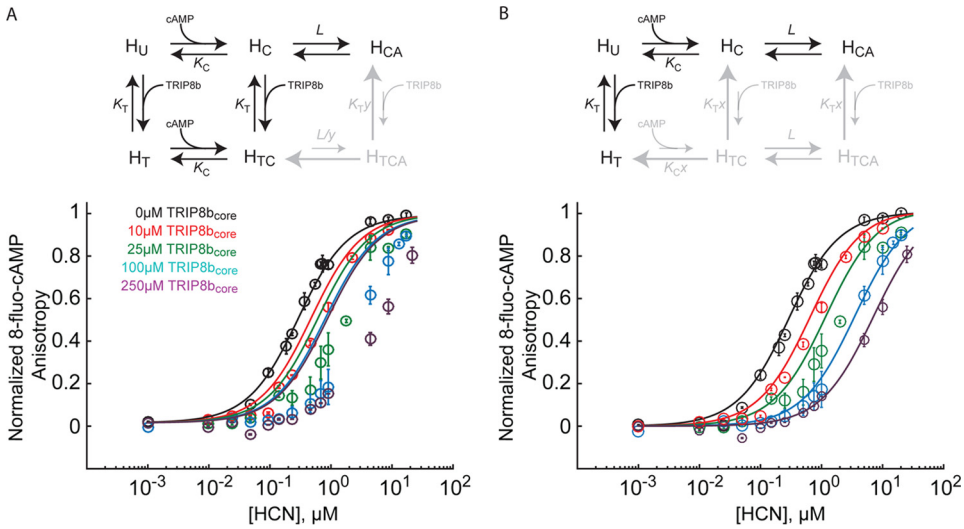

Figure 6. Data for cAMP binding to HCN2-CNBDxt in the presence of TRIP8b are best fit with a partial competition model. *A*, normalized fluorescence anisotropy data for 8-fluo-cAMP binding to HCN2-CNBDxt at difference concentrations of TRIP8b$_{core}$ fit with the noncompetitive model at the *top*. In this example, $y = 10{,}000$, making the H_{TCA} state essentially unpopulated. The fits are very poor. For the noncompetitive model, $K_C = 0.745$ μM, $K_T = 7.34$ μM, $L = 1.3$, and $y = 10{,}000$. *B*, normalized fluorescence anisotropy data for 8-fluo-cAMP binding to HCN2-CNBDxt fit with the partially competitive model at the *top*. Here, $x = 100$ resulted in a good fit to the data. For the competitive model, $K_C = 0.745$ μM, $K_T = 7.34$ μM, $L = 1.3$, and $x = 100$. The data are plotted as means ± S.E.

the context of our models, that an effect on binding is necessary and sufficient to allow TRI8b to antagonize the cAMP dependence of HCN channels.

To confirm our conclusion using an alternative approach, we again utilized DEER to measure the probability that the CNBD is in the active conformation. We performed DEER experiments that can distinguish between the two models for TRIP8b inhibition of cAMP regulation. The models make different predictions about the probability that HCN2-CNBDxt would be in the active *versus* resting states in the presence of both cAMP and TRIP8b. We calculated these probabilities for each model using 25 μM HCN2-CNBDxt and 1 mM cAMP and varied the concentration of TRIP8b. For the noncompetitive model, we assumed $y = 100$, and for the partially competitive model, we assumed $x = 100$. As shown in Fig. 7*A*, in the noncompetitive model, increasing the concentration of TRIP8b dramatically reduced the fraction of active CNBD molecules. However, in the partially competitive model, the fraction of CNBD molecules in the active state was insensitive to TRIP8b concentration.

Based on these simulations, we designed DEER experiments to further test which model best explains the mechanism of TRIP8b regulation of HCN channels. We replicated these model conditions in our DEER experiments, using 25 μM HCN2-CNBDxt and 1 mM 8-fluo-cAMP in each experiment. We performed DEER experiments in the absence and presence of 300 μM TRIP8b. At this concentration of TRIP8b, the two models make dramatically different predictions (Fig. 7*A*). The noncompetitive model predicts that this concentration of TRIP8b should have a large effect on the fraction of CNBD molecules in the active conformation, whereas the partially competitive model predicts that TRIP8b should have little effect. The result of the DEER experiments are shown in Fig. 7*B*. In the presence of 300 μM TRIP8b$_{core}$ and 1 mM 8-fluo-cAMP, the fraction of HCN2-CNBDxt in the active state is almost identical to that of the domain in the presence of 8-fluo-cAMP alone, consistent with the predictions made by the partially competitive model. These experiments were done using 8-fluo-cAMP to maintain consistency in the experiments throughout this study; however, supplemental Fig. S2 shows that qualitatively the same pattern is seen when using cAMP.

Discussion

TRIP8b has been shown to dramatically reduce the cAMP dependence of HCN channels (2, 3, 5, 8–10, 12). Binding of a small central region of TRIP8b (TRIP8b$_{core}$) to the CNBD of HCN channels is both necessary and sufficient for this effect (9, 10). However, the mechanism for this inhibition is still unclear. To better understand the mechanism, we considered two multistate models that represent the simplest possible mechanisms of inhibition. In the first mechanism, noncompetitive inhibition, TRIP8b binds to the CNBD of HCN channels and inhibits the conformational change associated with channel activation. This mechanism is perhaps most intuitive, given that the TRIP8b binding site is thought to involve moving parts of the CNBD (10, 11). In the second mechanism, partially competitive inhibition, TRIP8b and cAMP are competing for the same binding site on the CNBD. Although less intuitive, this mechanism suggests that the binding sites for cAMP and TRIP8b partially overlap or that the binding of one ligand distorts the binding site of the other (through a conformational change different from the one associated with channel activation). Fitting these models to cAMP binding data in the absence and presence of TRIP8b$_{core}$, we found that competition was both necessary and sufficient to fit our data.

Beyond suggesting that partial competition explained our binding data, the models we developed also made specific predictions about how the CNBD would change conformation in the presence of cAMP and TRIP8b. If the mechanism was partial competition, the model predicts that, in saturating cAMP,

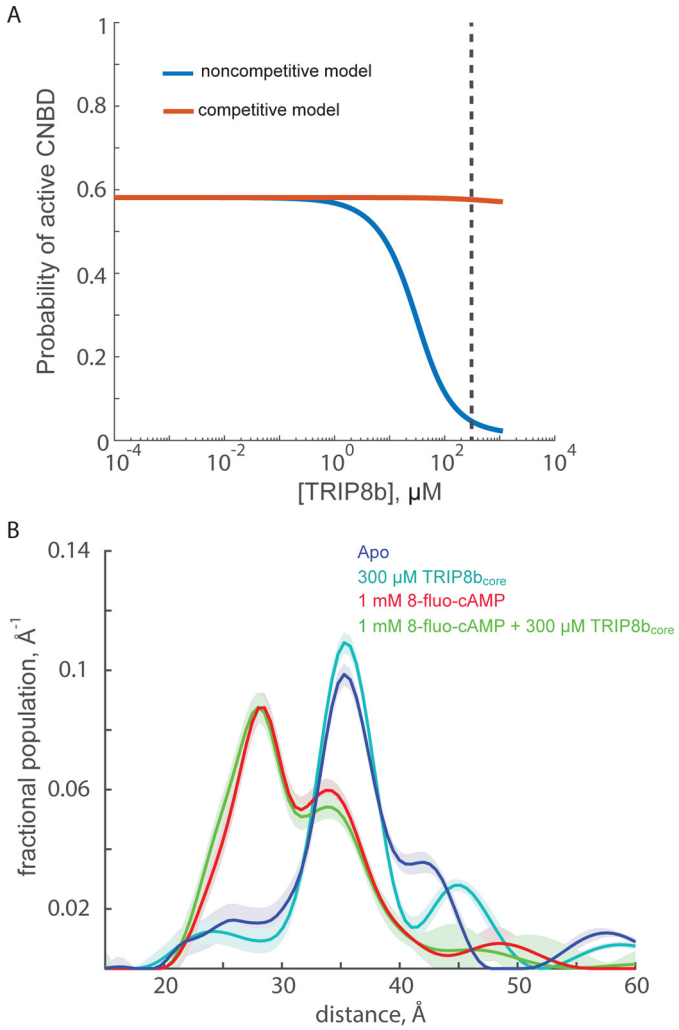

Figure 7. DEER data support the partial competition hypothesis. *A*, model predictions for the fraction of active CNBD molecules with 25 μM HCN2-CNBDxt and 1 mM cAMP as a function of TRIP8b concentration for both the noncompetitive and competitive models. For both models, $K_C = 0.745$ μM, $K_T = 7.34$ μM, and $L = 1.3$. For the noncompetitive model $y = 100$, and for the competitive model $x = 100$. The noncompetitive model (*blue line*) shows that the probability of finding the CNBD in the active state is strongly dependent on TRIP8b concentration. However, the partially competitive model (*red line*) shows that the probability of finding the CNBD in the active state is only weakly dependent on TRIP8b concentration. The *vertical dotted line* marks 300 μM TRIP8b$_{core}$. *B*, distance distributions of HCN2-CNBDxt S563C/A624C (*blue*), with 300 μM TRIP8b$_{core}$ (*cyan*), with 1 mM 8-fluo-cAMP (*red*), and with 1 mM 8-fluo-cAMP and 300 μM TRIP8b$_{core}$ (*green*).

adding a large amount of TRIP8bcore (300 μM) to HCN2-CNBDxt (25 μM) would have almost no effect on the conformational equilibrium between the resting and active states. On the other hand, if TRIP8b regulates HCN channels by a noncompetitive mechanism, the model predicts that under that same condition, there would be a dramatic reduction in the probability that HCN2-CNBDxt would undergo the conformational change into the active state. DEER provided us with a powerful technique to look at conformational equilibria in purified proteins. By measuring DEER distributions under the conditions that we modeled, we were able to show that TRIP8b had little effect on the probability that HCN2-CNBDxt would undergo the conformational change into the active state, confirming again that a partial competition model best fits the data.

NMR work from two groups also shed light on the mechanism of TRIP8b inhibition (10, 11). Both groups used chemical shift perturbation analysis to look at residues on the CNBD of HCN channels are likely to be involved in binding to TRIP8b. Although the two studies used different HCN isoforms (HCN2 and HCN4), the similarity in structures and inhibition by TRIP8b suggests that the interactions and mechanisms of inhibition will be similar (10, 11, 19). Overall, the two studies show similar chemical shift perturbations when TRIP8b is added to the CNBD of HCN. The residues that were most affected cluster in the C-helix, the cAMP-binding site, and the C-linker region, both regions that are involved in ligand binding and the subsequent conformational change. Interestingly, a new structure of the full human HCN1 channel shows two helices after the C-helix that are positioned in the region where TRIP8b binds to the channel and could also be involved in TRIP8b binding (20).

Previous studies have reached different conclusions about the mechanism of TRIP8b-dependent regulation of HCN channels. Using patch clamp electrophysiology, Hu *et al.* (9) perfused purified TRIP8b$_{core}$ onto membrane patches expressing HCN2 channels and measured the changes in the functional properties of the channels. They showed that TRIP8b reduced the maximal voltage shift caused by cAMP even at saturating concentrations of cAMP. In addition, they used a 12-state kinetic model to fit their data and concluded that the effect of TRIP8b on cAMP binding to the open state of the channels was larger than on cAMP binding to the closed state, suggesting an effect of TRIP8b on the allosteric opening transition. Overall, the authors concluded that TRIP8b is modulating HCN channels through a mechanism where TRIP8b binding allosterically reduces the affinity for cAMP, as well as alters the opening conformational transition (9). Work from another group used pulldown assays to show that increasing concentrations of cAMP or mutation of the cAMP-binding site reduces TRIP8b binding to the CNBD (5). From this the authors conclude that TRIP8b and cAMP are competing for the same binding site.

What explains the difference in conclusions between our current study and previous studies? The present study uses the HCN2-CNBDxt fragment that lacks the rest of the channel and the ability to tetramerize. It is possible that cAMP and TRIP8b may bind differently to the isolated fragment and that the precise mechanistic details could vary. Although we chose simple, physically intuitive models, we also cannot completely rule out that our conclusions may be somewhat model-dependent. It is worth pointing out that our results do not eliminate the possibility that TRIP8b affects both the conformational change of the CNBD, as well as the cAMP binding itself. The modeling only indicates that an ~100-fold increase in the dissociation constant for cAMP binding is sufficient to explain the change in cAMP binding to the CNBD in the presence of TRIP8b.

Although the data presented here suggest that TRIP8b and cAMP are in partial competition for binding to HCN channels, the structural mechanism for this competition is still unknown. NMR and DEER data have mapped an interface for these two proteins that includes the C-helix, C-linker, and cAMP-binding site (10). This leads us to hypothesize that TRIP8b binds along the C-helix of HCN channels and competes with a portion of

the cAMP-binding site or distorts the binding site by making interactions with the binding pocket, thus inhibiting the cyclic nucleotide dependence of these channel by acting like a partially competitive antagonist.

Experimental procedures

Molecular biology

All constructs used to express the HCN2 CNBD and TRIP8b fragments were subcloned into the pETM11 vector. The proteins were separated from the histidine tag by a tobacco etch virus (TEV) cleavable linker. $TRIP8b_{core}$ was derived from the murine TRIP8b(1a-4) isoform and contained residues 223–303 of that protein (9, 10). Murine HCN2-CNBDxt contained residues 488–640 (10). For EPR experiments, this construct was made in a cysteine-free background (10). Cysteine mutations were engineered into the constructs at the indicated positions using standard PCR-based methods. All constructs were confirmed with fluorescence-based automated sequencing. The cDNAs encoding the full-length murine HCN2 channel in the pGHE vectors were kindly provided by Steven Siegelbaum and Bina Santoro (Columbia University) (21). The TRIP8b cDNAs were provided by Dane Chetkovich (Northwestern University) (3).

Patch clamp recording

cRNA for HCN2 channels was transcribed using the mMessage Machine T7 transcription kit (Ambion) and expressed in *X. laevis* oocytes that were defolliculated and injected with the cRNA as previously described (22). The vitelline membranes were manually removed, and currents were recorded in the inside-out patch-clamp configuration (23) with an EPC-10 patch-clamp amplifier (HEKA Elektronik). HCN2 channels are known to run down upon patch excision because of phosphatidylinositol 4,5-bisphosphate depletion (24). Thus, we allowed 20–30 min for the HCN current from the patch to stabilize before starting the experiment. Patch pipettes were pulled from borosilicate glass and had resistances of 0.4–0.6 MΩ after fire polishing. The pipette and bath solutions for HCN2 recordings were as follows: 130 mM KCl, 3 mM HEPES, and 0.2 mM EDTA (pH 7.2). $TRIP8b_{core}$ and cAMP were added to these solutions at the concentrations indicated. The solutions were perfused onto the patches using a μflow low volume perfusion system (ALA Scientific Instruments). Patches were held at 0 mV, and HCN2 currents were elicited by applying a series of 2-s voltage steps ranging from −70 to −140 mV followed by a 1-s voltage pulse to −40 mV. The data were analyzed using Igor (Wavemetrics) and MATLAB (MathWorks).

Protein expression, purification, and spin labeling

For each protein expressed, the construct was transfected into BL21(DE3) cells. 2-Liter cultures of cells were grown at 37 °C to an optical density of 0.6–0.8. The cells were then induced with 1 mM isopropyl β-D-1-thiogalactopyranoside and grown overnight at 18 °C. After growth and expression, the cells were pelleted by centrifugation at 4,000 × *g* at 4 °C for 10 min and resuspended in 150 mM KCl and 30 mM HEPES at pH 7.4 (for HCN2-CNBDxt) or pH 8.5 (for $TRIP8b_{core}$). DNase at a final concentration of 5 μg/ml and two tablets of protease inhibitors (cOmplete EDTA-free; Roche) were added to the buffer. The resuspended cells were lysed by an Emulsiflex-C3 homogenizer (Avestin) and clarified by centrifugation at 186,000 × *g* at 4 °C for 45 min. The lysate was then purified on a Ni^{2+} affinity resin column (HisTrap HP; GE Healthcare). For most experiments, the octahistidine tag was removed by TEV protease cleavage overnight at 4 °C. For the biolayer interferometry experiments, the octahistidine tag was left on the amino terminus of HCN2-CNBDxt. For anisotropy and DEER experiments, the proteins were then labeled with 100 μM monobromobimane (mBBr) or MTSL (Toronto Research Chemicals), respectively, for 1 h at room temperature or 6–16 h at 4 °C. To remove the TEV protease and further purify the samples, the proteins were purified on an ion-exchange column. For HCN2 proteins, a cation-exchange column was used (HiTrap SP FF; GE Healthcare). For TRIP8b(1a-4) and for $TRIP8b_{core}$, an anion-exchange column (HiTrap Q HP; GE Healthcare) was used. The proteins were eluted with a KCl gradient from 15 mM to 1 M. Fractions with protein were pooled and concentrated using a 3-kDa molecular mass cutoff centrifugal filter (Vivaspin; General Electric). The samples were then buffer-exchanged into a 150 mM KCl, 30 mM Tris, pH 8.4, solution using a PD-10 column (GE Healthcare). For CW EPR and DEER experiments, the protein was buffer-exchanged into D_2O with 150 mM KCl, 30 mM Tris, pH 8.4, and 10% glycerol.

Fluorescence anisotropy

Fluorescence anisotropy was recorded using a Fluorolog 3 spectrofluorometer (Horiba, Jobin Yvon). The cAMP binding experiments utilized a fluorescent analog called 8-(2-[fluoresceinyl] aminoethylthio)adenosine-3′,5′-cyclic monophosphate (8-fluo-cAMP) (Biolog, Bremen, Germany). Anisotropy experiments with 390-nm (mBBr) or 494-nm (8-fluo-cAMP) excitation and 490-nm (mBBr) or 514-nm (8-fluo-cAMP) emission were performed as previously described (25). To estimate binding affinity, plots of the anisotropy *versus* total HCN2-CNBDxt concentration were fit using the following first-order reaction scheme,

$$R + A \leftrightarrow RA \quad \text{(Eq. 1)}$$

$$\text{Anistropy} = \alpha\left[\frac{(R_t + K_d + A_t) - \sqrt{(-R_t - K_d - A_t)^2 - 4R_tA_t}}{2}\right] + \beta \quad \text{(Eq. 2)}$$

where R, A, and RA are concentrations of the free receptor, ligand, and receptor-ligand complex, respectively. R_t and A_t are total receptor and ligand concentrations, K_d is the dissociation constant, and α and β are the scaling factor and offset factor, respectively.

Biolayer interferometry

Binding kinetics of $TRIP8b_{core}$ to the HCN2-CNBDxt were determined using the Octet Red 96 (ForteBio, Pall Life Sciences). Optical probes coated with Ni-NTA were loaded with an octahistidine-tagged HCN2-CNBDxt. All reaction solutions (200 μl) were loaded into black 96-well plates. The reaction

buffer was 150 mM KCl and 30 mM HEPES, pH 8.4. There was no binding of $TRIP8b_{core}$ to the unloaded probes. Binding kinetics of multiple concentrations of $TRIP8b_{core}$ was measured simultaneously using eight probes. The data were acquired using the software for the Octet Red 96 and then analyzed offline using a script written for Igor (Wavemetrics). Binding kinetics were fit using an equation for a simple bimolecular reaction,

$$F = \alpha \times [e^{(-([\text{TRIP8bcore}] \times k_{on} + k_{off}) \times t)}] + \beta \quad \text{(Eq. 3)}$$

where F is the signal from the Octet Red 96, k_{on} and k_{off} are the binding and unbinding rate constants, respectively, and α and β are the scaling factor and offset factor, respectively. The rate constants were fit globally using the global fit routine in Igor to come up with a single set of values that best fit the data at all the concentrations of $TRIP8b_{core}$. In addition, the binding kinetics for each concentration of $TRIP8b_{core}$ were fit with the following equation,

$$F = \alpha \times [e^{(-(k_{obs}) \times t)}] + \beta \quad \text{(Eq. 4)}$$

and the observed rate (k_{obs}) was plotted as a function of $TRIP8b_{core}$ concentration. This plot was then fit with the following equation,

$$k_{obs} = k_{on} \times [TRIP8b_{core}] + k_{off} \quad \text{(Eq. 5)}$$

as a second method for estimating k_{on} and k_{off}.

EPR data collection and analysis

Doubly spin-labeled HCN protein for intraprotein DEER measurements was diluted to ~50 μM. $TRIP8b_{core}$ or cAMP was added as indicated in the text. 50 μl of each protein sample was inserted into a 1.65-mm outer-diameter quartz tube (Sutter, Q165-115-10). In an attempt to trap the room temperature equilibrium conformational ensemble, samples were flash frozen by rapid placement into liquid nitrogen. This procedure is known to result in a narrower ensemble of spin label rotamers (16, 17).

DEER data were acquired on a 33–35 GHz Bruker ELEXSYS E580 spectrometer with an overcoupled dielectric resonator (Bruker EN5107D2, 34.1 GHz, Q-factor 300–700). Experiments were performed at 60 K using a liquid-helium cooling system (Oxford). The four-pulse, dead-time free DEER sequence $[(\pi/2)_{probe} - \tau_1 - (\pi)_{probe} - \tau_1 + t - (\pi)_{pump} - (\tau_2 - t) - (\pi)_{probe} - \tau_2]$ was used with 22-ns probe pulses and a 44-ns pump pulse. Pulse delays were 120 ns for τ_1 and 1800 ns for τ_2. The delay t was varied from −60 ns to between 1,800 and 4,000 ns, depending on the experiments, in 10-ns increments. The pump frequency matched the nitroxide spectral maximum. The probe frequency was centered in the resonator dip and was 62 MHz lower than the pump frequency. An eight-step phase cycling protocol combined with extensive averaging at a repetition time of 2 ms was used to collect data. The measurement time for each sample was 10–16 h.

DEER distance distributions were obtained using DeerAnalysis2013 (26). A homogeneous three-dimensional background was used for background correction. Time traces were converted to distance distributions using Tikhonov regularization, a model-free least-squares approach. The regularization parameter was optimized separately for each data set according to the L-curve criterion. To estimate errors associated with our measurement, the noise in the time domain traces was linearly transformed to the distance domain. The shaded error bands shown in the distance distributions correspond to two standard deviations of the time domain noise. Molecular graphics and analyses were performed with UCSF Chimera and PyMOL (27–29).

Modeling of $TRIP8b_{core}$ inhibition of cAMP binding to HCN2-CNBDxt

To distinguish between two mechanistic hypotheses for TRIP8b regulation of HCN channels, we created a six-state model to fit our binding data. The model is shown in Fig. 4 (*B* and *C*). The six states represent the following: H_U is the completely unbound HCN-CNBD, H_C is the cAMP bound HCN-CNBD in the resting conformation, H_{CA} is the cAMP bound HCN-CNBD in the active conformation, H_T is the TRIP8b bound HCN-CNBD, H_{TC} is the cAMP and TRIP8b bound HCN-CNBD in the resting state, and H_{TCA} is the cAMP and TRIP8b bound HCN-CNBD in the active state. A combination of fluorescence anisotropy, biolayer interferometry, and DEER experiments were used to determine binding affinities for cAMP and TRIP8b to HCN2-CNBDxt and to determine the equilibrium constant for the conformational change, L. We then varied the parameter x or y (see Fig. 4, *B* and *C*) to produce the best fit of each model to the cAMP binding data with different concentrations of $TRIP8b_{core}$. Igor was used to calculate the roots of the following equations.

$$H_{tot} = H_U + H_C + H_{CA} + H_T + H_{TC} + H_{TCA} \quad \text{(Eq. 6)}$$

$$C_{tot} = C + H_C + H_{CA} + H_{TC} + H_{TCA} \quad \text{(Eq. 7)}$$

$$T_{tot} = T + H_T + H_{TC}\text{v} + H_{TCA} \quad \text{(Eq. 8)}$$

$$K_C = \frac{H_U \times C}{H_C} \quad \text{(Eq. 9)}$$

$$K_T = \frac{H_U \times T}{H_T} \quad \text{(Eq. 10)}$$

$$L = \frac{H_{CA}}{H_C} \quad \text{(Eq. 11)}$$

For the noncompetitive model,

$$y = \frac{H_{CA} \times H_{TC}}{H_C \times H_{TCA}} \quad \text{(Eq. 12)}$$

For the competitive model,

$$x = \frac{H_C \times H_T}{H_U \times H_{TC}} \quad \text{(Eq. 13)}$$

where H_{tot}, C_{tot}, and T_{tot} are the total concentrations of HCN2-CNBDxt, cAMP, and $TRIP8b_{core}$, respectively, used in the experiment, and C and T are the concentrations of free cAMP, and $TRIP8b_{core}$, respectively. The other variables are defined in

Fig. 4*B*. For each set of equilibrium constants, we calculated the fraction of cAMP bound as a function of H_{tot} using the following equation.

$$\text{Fraction cAMP bound} = 1 - \frac{C}{C_{tot}} \quad \text{(Eq. 14)}$$

Statistics

The data were plotted as means ± S.E. Student's *t* test was used to determine significance at $p < 0.05$.

Author contributions—J. R. B. designed, conducted, analyzed experiments, and wrote the paper. H. A. D. designed, conducted, and analyzed experiments. W. N. Z. and S. S. analyzed experiments and wrote the paper.

Acknowledgments—We thank Dr. Tom Hinds for technical assistance and Dr. Ning Zheng for the use of the Octet Red96 system. Chimera is developed by the Resource of Biocomputing, Visualization, and Informatics at the University of California, San Francisco (supported by NIGMS, National Institutes of Health Grant P41GM103311).

References

1. Wainger, B. J., DeGennaro, M., Santoro, B., Siegelbaum, S. A., and Tibbs, G. R. (2001) Molecular mechanism of cAMP modulation of HCN pacemaker channels. *Nature* **411,** 805–810
2. Santoro, B., Piskorowski, R. A., Pian, P., Hu, L., Liu, H., and Siegelbaum, S. A. (2009) TRIP8b splice variants form a family of auxiliary subunits that regulate gating and trafficking of HCN channels in the brain. *Neuron.* **62,** 802–813
3. Lewis, A. S., Schwartz, E., Chan, C. S., Noam, Y., Shin, M., Wadman, W. J., Surmeier, D. J., Baram, T. Z., Macdonald, R. L., and Chetkovich, D. M. (2009) Alternatively spliced isoforms of TRIP8b differentially control h channel trafficking and function. *J. Neurosci.* **29,** 6250–6265
4. Piskorowski, R., Santoro, B., and Siegelbaum, S. A. (2011) TRIP8b splice forms act in concert to regulate the localization and expression of HCN1 channels in CA1 pyramidal neurons. *Neuron* **70,** 495–509
5. Han, Y., Noam, Y., Lewis, A. S., Gallagher, J. J., Wadman, W. J., Baram, T. Z., and Chetkovich, D. M. (2011) Trafficking and gating of hyperpolarization-activated cyclic nucleotide-gated channels are regulated by interaction with tetratricopeptide repeat-containing Rab8b-interacting protein (TRIP8b) and cyclic AMP at distinct sites. *J. Biol. Chem.* **286,** 20823–20834
6. Zolles, G., Wenzel, D., Bildl, W., Schulte, U., Hofmann, A., Müller, C. S., Thumfart, J.-O., Vlachos, A., Deller, T., Pfeifer, A., Fleischmann, B. K., Roeper, J., Fakler, B., and Klöcker, N. (2009) Association with the auxiliary subunit PEX5R/Trip8b controls responsiveness of HCN channels to cAMP and adrenergic stimulation. *Neuron* **62,** 814–825
7. Santoro, B., Wainger, B. J., and Siegelbaum, S. A. (2004) Regulation of HCN channel surface expression by a novel C-terminal protein-protein interaction. *J. Neurosci.* **24,** 10750–10762
8. Bankston, J. R., Camp, S. S., DiMaio, F., Lewis, A. S., Chetkovich, D. M., and Zagotta, W. N. (2012) Structure and stoichiometry of an accessory subunit TRIP8b interaction with hyperpolarization-activated cyclic nucleotide-gated channels. *Proc. Natl. Acad. Sci. U.S.A.* **109,** 7899–7904
9. Hu, L., Santoro, B., Saponaro, A., Liu, H., Moroni, A., and Siegelbaum, S. (2013) Binding of the auxiliary subunit TRIP8b to HCN channels shifts the mode of action of cAMP. *J. Gen. Physiol.* **142,** 599–612
10. DeBerg, H. A., Bankston, J. R., Rosenbaum, J. C., Brzovic, P. S., Zagotta, W. N., and Stoll, S. (2015) Structural mechanism for the regulation of HCN ion channels by the accessory protein TRIP8b. *Structure* **23,** 734–744
11. Saponaro, A., Pauleta, S. R., Cantini, F., Matzapetakis, M., Hammann, C., Donadoni, C., Hu, L., Thiel, G., Banci, L., Santoro, B., and Moroni, A. (2014) Structural basis for the mutual antagonism of cAMP and TRIP8b in regulating HCN channel function. *Proc. Natl. Acad. Sci. U.S.A.* **111,** 14577–14582
12. Santoro, B., Hu, L., Liu, H., Saponaro, A., Pian, P., Piskorowski, R. A., Moroni, A., and Siegelbaum, S. A. (2011) TRIP8b regulates HCN1 channel trafficking and gating through two distinct C-terminal interaction sites. *J. Neurosci.* **31,** 4074–4086
13. Puljung, M. C., DeBerg, H. A., Zagotta, W. N., and Stoll, S. (2014) Double electron-electron resonance reveals cAMP-induced conformational change in HCN channels. *Proc. Natl. Acad. Sci. U.S.A.* **111,** 9816–9821
14. DeBerg, H. A., Brzovic, P. S., Flynn, G. E., Zagotta, W. N., and Stoll, S. (2016) Structure and energetics of allosteric regulation of HCN2 ion channels by cyclic nucleotides. *J. Biol. Chem.* **291,** 371–381
15. Polyhach, Y., Bordignon, E., and Jeschke, G. (2011) Rotamer libraries of spin labelled cysteines for protein studies. *Phys. Chem. Chem. Phys.* **13,** 2356–2366
16. Jeschke, G. (2013) Conformational dynamics and distribution of nitroxide spin labels. *Prog. Nucl. Magn. Reson. Spectrosc.* **72,** 42–60
17. Georgieva, E. R., Roy, A. S., Grigoryants, V. M., Borbat, P. P., Earle, K. A., Scholes, C. P., and Freed, J. H. (2012) Effect of freezing conditions on distances and their distributions derived from double electron electron resonance (DEER): a study of doubly-spin-labeled T4 lysozyme. *J. Magn. Reson.* **216,** 69–77
18. Collauto, A., DeBerg, H. A., Kaufmann, R., Zagotta, W. N., Stoll, S., and Goldfarb, D. (2017) Rates and equilibrium constants of the ligand-induced conformational transition of an HCN ion channel protein domain determined by DEER spectroscopy. *Phys. Chem. Chem. Phys.* **19,** 15324–15334
19. Akimoto, M., Zhang, Z., Boulton, S., Selvaratnam, R., VanSchouwen, B., Gloyd, M., Accili, E. A., Lange, O. F., and Melacini, G. (2014) A mechanism for the auto-inhibition of hyperpolarization-activated cyclic nucleotide-gated (HCN) channel opening and its relief by cAMP. *J. Biol. Chem.* **289,** 22205–22220
20. Lee, C.-H., and MacKinnon, R. (2017) Structures of the human HCN1 hyperpolarization-activated channel. *Cell* **168,** 111–120
21. Santoro, B., Liu, D. T., Yao, H., Bartsch, D., Kandel, E. R., Siegelbaum, S. A., and Tibbs, G. R. (1998) Identification of a gene encoding a hyperpolarization-activated pacemaker channel of brain. *Cell* **93,** 717–729
22. Zagotta, W. N., Hoshi, T., and Aldrich, R. W. (1989) Gating of single Shaker potassium channels in *Drosophila* muscle and in *Xenopus* oocytes injected with Shaker mRNA. *Proc. Natl. Acad. Sci. U.S.A.* **86,** 7243–7247
23. Hamill, O. P., Marty, A., Neher, E., Sakmann, B., and Sigworth, F. J. (1981) Improved patch-clamp techniques for high-resolution current recording from cells and cell-free membrane patches. *Pflügers Arch.* **391,** 85–100
24. Pian, P., Bucchi, A., Robinson, R. B., and Siegelbaum, S. A. (2006) Regulation of gating and rundown of HCN hyperpolarization-activated channels by exogenous and endogenous PIP_2. *J. Gen. Physiol.* **128,** 593–604
25. Rossi, A. M., and Taylor, C. W. (2011) Analysis of protein-ligand interactions by fluorescence polarization. *Nat. Protoc.* **6,** 365–387
26. Jeschke, G., Chechik, V., Ionita, P., and Godt, A. (2006) DeerAnalysis2006: a comprehensive software package for analyzing pulsed ELDOR data. *Appl. Magn. Reson.* **30,** 473–498
27. Meng, E. C., Pettersen, E. F., Couch, G. S., Huang, C. C., and Ferrin, T. E. (2006) Tools for integrated sequence-structure analysis with UCSF Chimera. *BMC Bioinformatics* **7,** 339
28. Pettersen, E. F., Goddard, T. D., Huang, C. C., Couch, G. S., Greenblatt, D. M., Meng, E. C., and Ferrin, T. E. (2004) UCSF Chimera: a visualization system for exploratory research and analysis. *J. Comput. Chem.* **25,** 1605–1612
29. DeLano, W. L. (2012) *The PyMOL Molecular Graphics System*, version 1.5.0.1, Schroedinger, LLC, New York
30. Zagotta, W. N., Olivier, N. B., Black, K. D., Young, E. C., Olson, R., and Gouaux, E. (2003) Structural basis for modulation and agonist specificity of HCN pacemaker channels. *Nature* **425,** 200–205